canonical DNA damage checkpoint pathways were hyperactivated (2, 11). By contrast, Gari et al. treated cells with hydroxyurea to deplete deoxynucleotide pools, and found that in the absence of MMS19, cells could not enter S phase of the cell division cycle (could not replicate DNA), and consequently did not elicit a DNA damage checkpoint signal (1, 12). Thus, in the study by Stehling et al., DNA repair was compromised because of reduced MMS19 synthesis, whereas in the study by Gari et al., DNA replication was compromised.

It is not yet clear how MMS19 recognizes the apoproteins it serves, nor whether it directly hands over Fe-S clusters to recipient proteins. There are Fe-S proteins that are not served by MMS19, but depend on the CIA complex, and those might be served by undiscovered MMS19-like adaptors. A more fundamental question is why so many DNA enzymes require Fe-S clusters. It seems dangerous to place iron so close to DNA, where it could potentially unleash reactive oxygen species and damage the nucleotides. Are the Fe-S proteins simply an evolutionary artifact that cannot be removed by selection, or do they serve some other purpose, such as sensing aberrant DNA structures (13)?

An increase in yeast nuclear genome instability was associated with mitochondrial defects (14), suggesting that mitochondrial dysfunction inhibited the production of Fe-S cluster–containing proteins required for genome integrity. The findings of Gari et al. and Stehling et al. offer further tools to test this hypothesis. In addition, gene mutations in several of the DNA repair and replication proteins serviced by MMS19 have been associated with various cancers (15). Could it be that MMS19 and its prospective associates serve as another set of oncogenic targets?

References and Notes
1. K. Gari et al., Science 337, 243 (2012); 10.1126/science.1219664.
2. O. Stehling et al., Science 337, 195 (2012); 10.1126/science.1219723.
3. T. A. Rouault, Dis. Model. Mech. 5, 155 (2012).
4. M. F. White, M. S. Dillingham, Curr. Opin. Struct. Biol. 22, 94 (2012).
5. J. A. Imlay, Annu. Rev. Biochem. 77, 755 (2008).
6. A. Sheftel, O. Stehling, R. Lill, Trends Endocrinol. Metab. 21, 302 (2010).
7. R. P. Cunningham et al., Biochemistry 28, 4450 (1989).
8. D. J. A. Netz et al., Nat. Chem. Biol. 8, 125 (2012).
9. L. Prakash, S. Prakash, Genetics 86, 33 (1977).
10. J. Rudolf et al., Mol. Cell 23, 801 (2006).
11. A. Pellicioli et al., EMBO J. 18, 6561 (1999).
12. Y. Sanchez et al., Science 286, 1166 (1999).
13. C. A. Romano et al., Biochemistry 50, 6133 (2011).
14. J. R. Veatch, M. A. McMurray, Z. W. Nelson, D. E. Gottschling, Cell 137, 1247 (2009).
15. Y. Wu, R. M. Brosh Jr., Nucleic Acids Res. 40, 4247 (2012).

MATERIALS SCIENCE

Driving Dislocations in Graphene

Luis L. Bonilla[1] and Ana Carpio[2]

Electron microscopy has revealed time-resolved glide and climb motion of dislocations in graphene and imaged their strain and rotation fields.

The movement of dislocations in crystals—defects such as an extra halfplane of atoms—can determine the strength of a material and how it will deform under a load, and how it accommodates strain (1). In most materials, tracking the movement of dislocations in three dimensions requires analysis of high-resolution transmission electron microscopy (TEM) images. Tracking atomic positions in graphene, a two-dimensional material, could simplify such studies, and on page 209 of this issue, Warner et al. (2) use a sophisticated TEM technique to see, create, and move dislocations in suspended graphene. These results can help guide efforts to improve our theoretical understanding of how defect motion affects the mechanical properties of materials.

In graphene, mechanical characteristics can have striking consequences for its electronic properties. For example, strains may induce strong pseudo-magnetic fields and Landau levels (3), whereas vacancies and point defects produce paramagnetism (4). Special grain boundaries—the interfaces between crystalline domains—may be used to filter electrons from different graphene "valleys" (different conduction bands for charge carriers) used in so-called "valleytronic" devices (5).

In the experiments performed by Warner et al., the electrons used for imaging were accelerated at low voltage so that they could not knock atoms off the graphene lattice (the maximum energy transferred from beam electrons is less than 17 eV at voltages lower than 90 kV). However, these energies were sufficient to rotate carbon-carbon (C–C) bonds, create defects, and knock atoms off defective sites. These defects are the cores of dislocations in the graphene lattice (6). For instance, a 90° C–C bond rotation requires
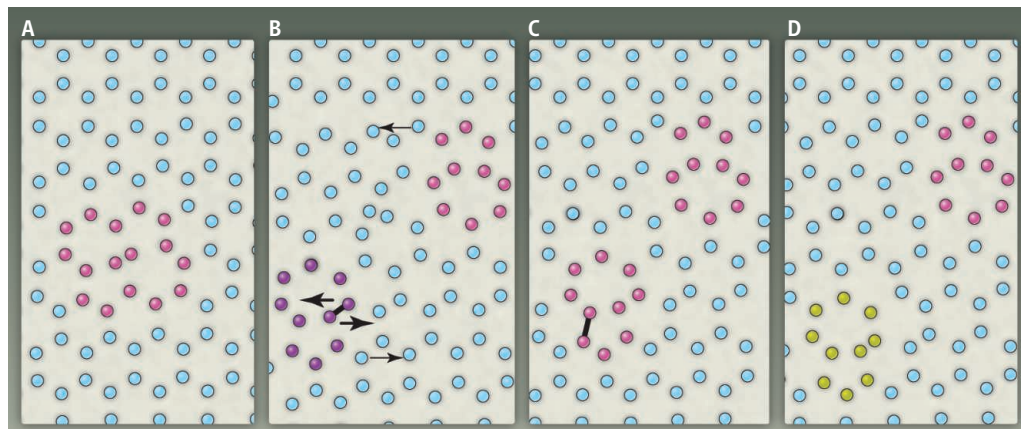
Driving dislocations. (**A**) A Stone-Wales defect (red) is shown in a graphene lattice (blue). (**B**) Dislocations are characterized by Burgers vectors (thin arrows), and the indicated pentagon-heptagon dislocations form from a dipole with Burgers vectors pointing in opposite directions along a primitive lattice direction (the horizontal axis). Warner et al. show that dislocations can advance parallel to their Burgers vector (glide) or in a different direction (climb), provided the electrons from the TEM beam can supply atoms with sufficient energy to overcome the corresponding energy barriers. Glide to the right involves moving two atoms as indicated by the thick arrows. (**C**) Configuration after dislocation glide. If the TEM beam knocks the marked atoms off, the left dislocation climbs vertically downward. (**D**) Resulting configuration after dislocation climb.

[1]Fluid Dynamics, Nanoscience and Industrial Mathematics Institute, Universidad Carlos III de Madrid, 28911 Leganes, Spain. [2]Applied Mathematics, Universidad Complutense de Madrid, 28040 Madrid, Spain. E-mail: ana_carpio@mat.ucm.es; bonilla@ing.uc3m.es

9.2 eV and transforms four hexagons in the pristine lattice into a ring comprising two pentagons and two heptagons, a Stone-Wales defect (SWD) (see the figure, panel A).

The SWD is a not a single dislocation but a dipole formed by two dislocations (the pentagon-heptagon pairs). The distortion of a lattice caused by a dislocation is described by a Burgers vector, and the SWD is a dipole because the Burgers vectors are of equal length and antiparallel. To revert back to the pristine, stress-free lattice, a SWD needs to be activated by about 4 eV, much less than the maximum energy the TEM can transfer to carbon atoms. In fact, the first TEM observations with reasonable atomic resolution revealed SWDs that disappeared within 4 s after their creation (7).

Under sufficient applied shear stress, a SWD splits into its two component dislocations that then glide apart [(6); see (8) for experimental evidence] (see the figure, panel B). From a pristine lattice, irradiation can create other dislocation pairs with zero overall Burgers vector. For example, nonagon-pentagon and pentagon-octagon-pentagon defects are the cores of vacancy and divacancy dislocation dipoles, respectively, created by the loss of one or two carbon atoms (6). More complicated defect rings and dynamics have also been observed (7–9).

Warner et al. have imaged dislocation dynamics in graphene in real time. They observed one dislocation in a dipole that glided one lattice constant toward the other along the direction marked by its Burgers vector. Later, it climbed another lattice constant away moving perpendicular to its Burgers vector (see the figure, panels C and D). The glide motion requires only atomic bond rotation (about 5 eV), whereas climbing involves removal of two atoms. The latter action has a higher energy cost (9 to 12 eV), and this energy is provided by the electrons from the TEM beam. The authors used density functional theory (DFT) to calculate the energy of defects located at different positions in the lattice once atoms have relaxed to a state compatible with boundary conditions and external stress constraints. Configurations that cost energy within the range provided by the TEM beam are plausible.

Despite DFT calculations showing that dislocation motion is consistent with energy barriers overcome by TEM irradiation, it remains unclear why dislocations move the way they do. What is the interplay among dislocations, strains, and irradiation? There are no complete theories of dislocation dynamics in graphene, although existing models based on discrete (6) or continuous elasticity

(10) could be a starting point. Future theories should also consider that strain fields (maps of the extent of compressive and tensile strain) around dislocations differ from those given by classical elasticity with line singularities (1). Using geometric phase analysis, Warner et al. have mapped dislocation strain fields. Formulas inspired by the semicontinuous Peierls-Nabarro model (1) give a better description than classical isotropic elasticity of strains at the dislocation cores. Furthermore, the lattice is rotated quite appreciably at the cores. These maps of strain and rotation fields could give additional clues about dislocation core structure.

Warner et al. have characterized dislocation motion in TEM-irradiated graphene with unprecedented accuracy. Their results should stimulate theory and experiments alike, as they offer the opportunity to understand plastic deformation in nanoscale materials. At the micrometer scale, there are effective computational theories of line dislocations that rely on empirical rules for dislocation interaction and motion (11).

Besides bridging the gap with the nanoscale, graphene could offer a benchmark for a quantitative theory of irradiation-driven dislocation dynamics. In addition, controlling electronic properties in graphene through strain engineering is a promising concept (3, 12). In this respect, learning how to produce appropriate dislocations and control their motion will be quite important.

References
1. J. P. Hirth, J. Lothe, *Theory of Dislocations* (Wiley, New York, ed. 2, 1982).
2. J. H. Warner et al., *Science* **337**, 209 (2012).
3. N. Levy et al., *Science* **329**, 544 (2010).
4. R. R. Nair et al., *Nat. Phys.* **8**, 199 (2012).
5. D. Gunlycke, C. T. White, *Phys. Rev. Lett.* **106**, 136806 (2011).
6. A. Carpio, L. L. Bonilla, *Phys. Rev. B* **78**, 085406 (2008).
7. J. C. Meyer et al., *Nano Lett.* **8**, 3582 (2008).
8. C. Gómez-Navarro et al., *Nano Lett.* **10**, 1144 (2010).
9. J. Kotakoski et al., *Phys. Rev. B* **83**, 245420 (2011).
10. S. Chen, D. C. Chrzan, *Phys. Rev. B* **84**, 214103 (2011).
11. V. V. Bulatov, W. Cai, *Computer Simulations of Dislocations* (Oxford Univ. Press, Oxford, 2006).
12. F. Guinea, M. I. Katsnelson, A. K. Geim, *Nat. Phys.* **6**, 30 (2010).

ECOLOGY

Amazonian Extinction Debts

Thiago F. Rangel

How many species are headed for extinction as a result of past and future deforestation in the Brazilian Amazon?

Habitat loss, climate change, and invasive species are the main drivers of the ongoing biodiversity crisis. These human-induced processes may have boosted the background rate of species extinction by 100 to 1000 times (1). However, species do not go extinct immediately when their habitat shrinks, climate changes beyond their tolerance limit, or an invasive species spreads. It may take several generations after an initial impact before the last individual of a species is gone. Conservation biologists are trying to estimate the time lag between habitat perturbation and species extinction. By inverting the reasoning, one can also estimate how many species are headed toward extinction as a function of past and current anthropogenic interference, the "extinction debt" (see the figure) (2). On page 228 of this issue, Wearn

Department of Ecology, Federal University of Goiás, CxP. 131, Goiânia, Goiás, Brazil 74970–001. E-mail: thiagorangel@icb.ufg.br

et al. (3) apply this approach to the Brazilian rainforest.

The authors tackle an important but challenging question: Across the Brazilian Amazon, how many species will be lost from at least part of their historical distribution as a consequence of past and future deforestation? The starting point for answering this question is the assumption that larger areas of old-growth forest habitat should harbor more species than smaller areas, an example of the "species-area relationship" (4). Deforestation reduces forest cover and available habitat area, consequently extirpating some native species not only from the impacted area but also from the remaining forest as populations fall below viability thresholds.

Wearn et al. used cutting-edge statistical tools to devise a novel strategy to estimate the expected number of local species extinctions as a function of the extent of habitat loss. In contrast to the modest record of local extinction across the Brazilian Amazon so far, their findings suggest that more than 80% of the

Published by AAAS